PHYSICAL REVIEW C **89**, 011307(R) (2014)

# Constraints on Skyrme equations of state from properties of doubly magic nuclei and *ab initio* calculations of low-density neutron matter

B. Alex Brown[1] and A. Schwenk[2,3]

[1]*Department of Physics and Astronom and National Superconducting Cyclotron Laboratory, Michigan State University, East Lansing, Michigan 48824-1321, USA*

[2]*ExtreMe Matter Institute EMMI, GSI Helmholtzzentrum für Schwerionenforschung GmbH, 64291 Darmstadt, Germany*

[3]*Institut für Kernphysik, Technische Universität Darmstadt, 64289 Darmstadt, Germany*

(Received 20 November 2013; published 30 January 2014)

We use properties of doubly magic nuclei and *ab initio* calculations of low-density neutron matter to constrain Skyrme equations of state for neutron-rich conditions. All of these properties are consistent with a Skyrme functional form and a neutron-matter equation of state that depends on three parameters. With a reasonable range for the neutron-matter effective mass, the values of the two other Skyrme parameters are well constrained. This leads to predictions for other quantities. The neutron skins for $^{208}$Pb and $^{48}$Ca are predicted to be 0.182(12) and 0.173(5) fm, respectively. Other results including the dipole polarizability are discussed.

DOI: 10.1103/PhysRevC.89.011307 PACS number(s): 21.10.Dr, 21.30.Fe, 21.60.Jz, 21.65.−f

The properties of the neutron equation of state (EOS) are important for understanding neutron skins and neutron stars [1–3]. Recently, an extensive study was performed on the constraints on Skyrme energy-density functionals (EDFs) provided by the properties of nuclear matter [4]. The standard form and the parameters of the Skyrme functional are given in Ref. [4]. Out of several hundred Skyrme EDFs, the 16 given in Table VI of Ref. [4], called the CSkP set, best reproduced a selected set of empirical nuclear matter properties. Five of these were eliminated [4] since they gave transitions to spin-ordered matter around densities of $\rho = 0.25$ fm$^{-3}$. One of the remainder (LNS) was unstable for finite nuclei. The remaining ten are those given in Table I and are labeled with their names and orders in Table VI of Ref. [4]. To this list, we add the commonly used SLy4 [5] and SkM* [6] functionals. These 12 EDFs cover a reasonable range of values for the symmetric-nuclear-matter effective mass ($m^*/m =$ 0.70–1.00) and incompressibility ($K_m =$ 212–242 MeV) as compared to values extracted from the energy of the giant monopole resonances ($K_m =$ 217–230 MeV) [7].

In Ref. [8], these 12 EDFs were refined by a fit to properties of the doubly magic nuclei $^{16}$O, $^{24}$O, $^{34}$Si, $^{40}$Ca, $^{48}$Ca, $^{48}$Ni, $^{68}$Ni, $^{88}$Sr, $^{100}$Sn, $^{132}$Sn, and $^{208}$Pb. The properties included binding energies, single-particle energies [9], root-mean-square (rms) charge radii, and rms neutron radii. The most experimentally uncertain of these are the rms neutron radii. With a fixed value for the neutron rms radius of $^{208}$Pb, the $t_0$, $t_1$, $t_2$, $t_3$, $x_0$, $x_3$, and $W$ (the spin-orbit strength) Skyrme parameters are well determined.

When the neutron skin of $^{208}$Pb is allowed to vary over the range of $R_{np} = \sqrt{\langle r_n^2\rangle} - \sqrt{\langle r_p^2\rangle} = 0.16$ to 0.24 fm, all of the EDFs cross at a value of the neutron density of about 0.10 fm$^{-3}$ with a value of $E/N = 11.3(8)$ MeV [8]. The slope at this point depends on the neutron skin [1,8]. The resulting neutron EOSs are shown here in Fig. 1. They are compared with the upper and lower values of the range from next-to-next-to-next-to-leading order (N$^3$LO) calculations of neutron matter [10,11] (the dashes lines in Fig. 1). We observe that the Skyrme EOSs obtained with a neutron skin of 0.20 fm are in best agreement with the theoretical N$^3$LO range.

In this Rapid Communication, we follow up on this observation and investigate, as additional constraints, the results from *ab initio* calculations of neutron matter. We simultaneously fit the experimental properties of doubly magic nuclei and the theoretical properties of low-density neutron matter. We do not include any data on the neutron radii of nuclei. Rather, as a result of the simultaneous fit, we will be able make predictions for the neutron EOS and properties associated with it, such as the neutron radii.

We include theoretical data points for the neutron-matter energy at three densities $\rho_n = 0.01$, 0.02, and 0.04 fm$^{-3}$. The range for the energy per particle is based on the recent N$^3$LO calculations that include two-, three-, and four-nucleon interactions in chiral effective field theory (EFT) [10,11] where the next-to-next-to-leading order (N$^2$LO) energies and the results with renormalization-group-evolved interactions [3,12] also are within this range. In addition, in the energy range, we include the results of first quantum Monte Carlo (QMC) calculations with local chiral EFT interactions at next-to-leading order (NLO) and N$^2$LO [13] (without three-nucleon forces, which are small at low densities). At the lowest density point $\rho_n = 0.01$ fm$^{-3}$, the energy range is

$$[E/N](\rho_n = 0.010\ \text{fm}^{-3}) = 3.00(13)\ \text{MeV}, \qquad (1)$$

which overlaps with the results from NLO lattice simulations that yield around 3.1 MeV [14]. At the second point $\rho_n =$ 0.02 fm$^{-3}$, the N$^3$LO range is $E/N =$ 4.14–4.34 MeV, and the chiral QMC range is 4.39–4.60 MeV. These overlap with the variational calculations of Akmal *et al.* based on the Argonne $v_{18}$ $NN$ and the Urbana IX (UIX) $3N$ potentials that give 4.35–4.45 MeV where the range is due to the inclusion of boost corrections [15]. In addition, we consider the auxiliary field diffusion Monte Carlo (AFDMC) results based on the Argonne $v_8'$ $NN$ and the same UIX $3N$ forces [16]. Extrapolating these from their lowest density result at $\rho_n = 0.04$ fm$^{-3}$ using their fits gives around 4.6 MeV.

 

TABLE I. Properties of the fitted Skyrme functionals. The effective mass $m_n^*/m$ in neutron matter at $\rho_n = 0.10$ fm$^{-3}$ is constrained to be 0.9 in the first part of the table and 1.0 in the second part. The symmetry energy $J$, its density derivative $L$, the symmetry-energy incompressibility $K_s$, the symmetric-nuclear-matter incompressibility $K_m$, and effective mass $m^*/m$ are evaluated at $\rho = 0.16$ fm$^{-3}$. The mean value is from the entire set, and the best value (b) is for the six cases that give the best fit to the data.

| Name | | $\sigma$ | $m_n^*/m$ | $\chi^2$ | $K_m$ (MeV) | $m^*/m$ | $a_n$ (MeV fm$^3$) | $b_n$ (MeV fm$^{3\gamma}$) | $d_n$ (MeV fm$^5$) | $J$ (MeV) | $L$ (MeV) | $K_s$ (MeV) | $R_{np}$ (fm) $^{208}$Pb | $R_{np}$ (fm) $^{48}$Ca |
|---|---|---|---|---|---|---|---|---|---|---|---|---|---|---|
| KDE0v1 | $s3$ | 1/6 | 0.90 | 1.81 | 216 | 0.79 | −455 | 422 | 145 | 34.9 | 61 | −130 | 0.192 | 0.172 |
| NRAPR | $s6$ | 0.14 | 0.90 | 2.60 | 225 | 0.85 | −534 | 509 | 133 | 35.1 | 61 | −142 | 0.193 | 0.178 |
| Ska25 | $s7$ | 0.25 | 0.90 | 0.91 (b) | 219 | 0.99 | −360 | 328 | 122 | 32.5 | 51 | −138 | 0.176 | 0.170 |
| Ska35 | $s8$ | 0.35 | 0.90 | 0.80 (b) | 244 | 1.00 | −317 | 315 | 123 | 32.8 | 54 | −144 | 0.180 | 0.172 |
| SKRA | $s9$ | 0.14 | 0.90 | 1.64 | 212 | 0.79 | −504 | 463 | 138 | 33.7 | 55 | −139 | 0.181 | 0.172 |
| SkT1 | $s10$ | 1/3 | 0.90 | 0.84 (b) | 242 | 0.97 | −324 | 326 | 124 | 33.3 | 56 | −140 | 0.183 | 0.172 |
| SkT2 | $s11$ | 1/3 | 0.90 | 0.86 (b) | 242 | 0.97 | −331 | 338 | 125 | 33.5 | 58 | −135 | 0.186 | 0.174 |
| SkT3 | $s12$ | 1/3 | 0.90 | 0.80 (b) | 241 | 0.98 | −322 | 314 | 134 | 32.7 | 53 | −144 | 0.179 | 0.172 |
| SQMC750 | $s15$ | 1/6 | 0.90 | 2.41 | 228 | 0.71 | −467 | 447 | 123 | 34.8 | 59 | −148 | 0.190 | 0.176 |
| SV-sym32 | $s16$ | 0.30 | 0.90 | 0.86 (b) | 237 | 0.91 | −335 | 313 | 123 | 32.3 | 51 | −148 | 0.176 | 0.174 |
| SLy4 | $s17$ | 1/6 | 0.90 | 1.97 | 224 | 0.70 | −450 | 412 | 136 | 34.1 | 56 | −145 | 0.184 | 0.174 |
| SkM* | $s18$ | 1/6 | 0.90 | 1.69 | 218 | 0.78 | −473 | 450 | 120 | 34.2 | 58 | −139 | 0.187 | 0.175 |
| Mean | | | | | | | | | | 33.8(13) | 56(5) | −138(8) | 0.184(9) | 0.174(4) |
| Mean (b) | | | | | | | | | | 32.9(4) | 54(4) | −141(4) | 0.180(4) | 0.172(2) |
| Ska25 | $s7$ | 0.25 | 1.00 | 0.85 (b) | 218 | 0.99 | −386 | 424 | 2 | 32.6 | 48 | −165 | 0.173 | 0.168 |
| Ska35 | $s8$ | 0.35 | 1.00 | 0.73 (b) | 244 | 1.00 | −333 | 419 | −3 | 33.1 | 53 | −165 | 0.179 | 0.171 |
| SkT1 | $s10$ | 1/3 | 0.99 | 0.76 (b) | 241 | 0.97 | −341 | 423 | 0 | 33.4 | 53 | −163 | 0.181 | 0.170 |
| SkT2 | $s11$ | 1/3 | 1.00 | 0.76 (b) | 230 | 0.97 | −338 | 413 | 4 | 33.1 | 52 | −164 | 0.179 | 0.170 |
| SkT3 | $s12$ | 1/3 | 1.00 | 0.73 (b) | 241 | 0.98 | −337 | 408 | 3 | 32.8 | 50 | −166 | 0.176 | 0.170 |
| SV-sym32 | $s16$ | 0.30 | 1.02 | 1.04 (b) | 242 | 0.91 | −364 | 450 | −21 | 33.4 | 51 | −176 | 0.178 | 0.173 |
| Mean (b) | | | | | | | | | | 33.0(4) | 50(3) | −170(7) | 0.178(4) | 0.171(3) |
| Overall | | | | | | | | | | 33.1(20) | 52(9) | −180(40) | 0.182(12) | 0.173(5) |

Therefore, we adopt, as a conservative range for the energy per particle at $\rho_n = 0.02$ fm$^{-3}$,

$$[E/N](\rho_n = 0.020 \text{ fm}^{-3}) = 4.37(23) \text{ MeV}. \quad (2)$$

At the density $\rho_n = 0.04$ fm$^{-3}$, the combined chiral EFT range is 5.40–6.65 MeV, which overlaps with the results of Akmal *et al.* that give 6.23–6.45 MeV, whereas the AFDMC results are 6.79(1) MeV. Therefore, we take

$$[E/N](\rho_n = 0.030 \text{ fm}^{-3}) = 6.1(7) \text{ MeV}. \quad (3)$$

Starting with the parameters given in Table VI of Ref. [4], we refit $t_0$, $t_1$, $t_2$, $t_3$, $x_0$, $x_3$, and $W$ to the doubly magic data and these three theoretical low-density neutron EOS values. There is no constraint on the neutron skin in the fit. These seven Skyrme parameters are all well determined by the fit. The EOS results for the 12 EDFs are shown in the bottom panel of Fig. 2 with the numerical results for the parameters given in Table I. The six "best-fit" results corresponding to those with a symmetric-nuclear-matter effective mass near unity are shown in the middle panel of Fig. 2. Inclusion of the theoretical points for low density does not give a significant increase in the $\chi^2$ for the fit compared to those from fits to the nuclear data alone [8]. We find that the theoretical points for low density can be reproduced within their error bars with all 12 of the EDFs and with similar good results for the properties of doubly magic nuclei. Furthermore, the addition of the low-density points is enough to constrain the Skyrme parameters needed for the neutron EOS. This leads to the predictions for the EOS properties and neutron skins for $^{208}$Pb and $^{48}$Ca given in Table I.

In Ref. [4], some of the Skyrme EDFs were eliminated because their neutron-matter effective mass was not less than unity. But as shown in Ref. [8], one can include the neutron-matter effective mass in the fit by allowing the $x_1$ or $x_2$ Skyrme parameters to vary, and this was used to set the neutron-matter effective mass to be 0.9 at a density of 0.10 fm$^{-3}$. In this Rapid Communication, we reconsider the value and consequence of the neutron-matter effective mass based on theoretical considerations. At low densities, the neutron-matter effective mass is close to $m_n^*/m \approx 1.0$. Calculations based on chiral EFT two- and three-nucleon interactions lead to a range of $m_n^*/m = 1.0$–$1.1$ (see Fig. 6 of Ref. [12]), and renormalization-group calculations of the Fermi-liquid parameters [17] give $m_n^*/m \approx 1.0$ up to densities of $\rho_n \lesssim 0.1$ fm$^{-3}$. An effective mass close to the bare mass or slightly increased also is expected from the unitary regime of neutron matter at very low densities [18].

To study the importance of the neutron-matter effective mass, we refit the six "best-fit" EDFs with a constraint that the neutron-matter effective mass is unity. The results are shown in the second part of Table I and in the top of Fig. 2. The last line of Table I shows the results and errors that include a variation of 0.9–1.1 for the neutron-matter effective mass. The variation in this range leads to a small change in the neutron skins. The largest uncertainty is for the symmetry-energy incompressibility $K_s$.

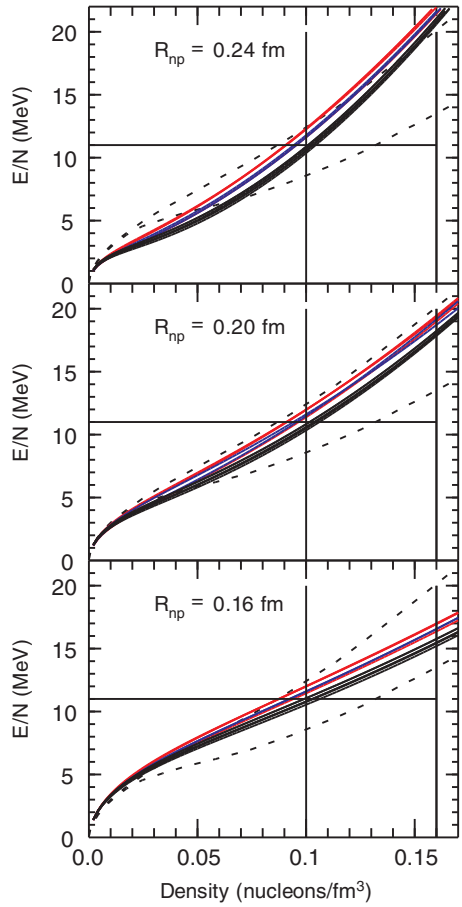


FIG. 1. (Color online) The neutron EOS with $m_n^*/m = 0.90$ and with $R_{np}$ fixed at 0.16, 0.20, and 0.24 fm compared to the N$^3$LO neutron-matter band from Ref. [10,11] (dashed lines). The black lines are those with symmetric-nuclear matter values of $m^*/m \approx 1.0$, and the red lines are those with $m^*/m = 0.70$–$0.85$. The blue lines are for SLy4 and SkM*.

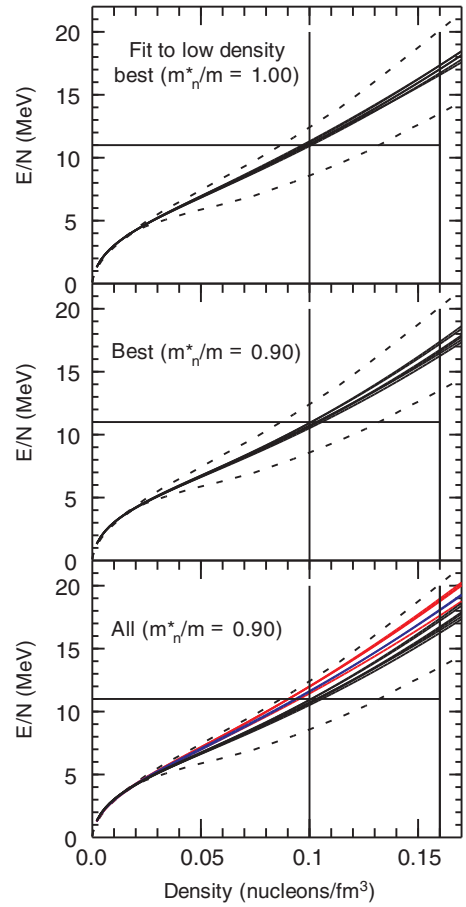


FIG. 2. (Color online) The neutron EOS from Skyrme fits that include points from *ab initio* calculations of low-density neutron matter, compared to the N$^3$LO neutron-matter band from Ref. [10,11] (dashed lines). The black lines are those with symmetric-nuclear matter values of $m^*/m \approx 1.0$, and the red lines are those with $m^*/m = 0.70$–$0.85$. The blue lines are for SLy4 and SkM*.

The Skyrme neutron EOS is given by the analytical expression,

$$[E/N](\rho) = a_n\rho + b_n\rho^{\gamma} + c_n\rho^{2/3} + d_n\rho^{5/3}, \qquad (4)$$

where $\gamma = 1 + \sigma$ and $a_n$, $b_n$, $c_n$, and $d_n$ are constants that depend on the Skyrme parameters. The first term is from the $\delta$-function part that depends on $t_0$ and $x_0$, the second term is from the density-dependent part that depends on $t_3$ and $x_3$, the third term is the Fermi-gas kinetic energy, and the fourth term depends on $t_1$, $t_2$, $x_1$, and $x_2$. The neutron-matter effective mass is given by

$$\frac{m_n^*(\rho)}{m} = \frac{c_n}{c_b + d_n\rho}. \qquad (5)$$

The very low-density results for one of the "best-fit" cases with a neutron-matter effective mass of unity are shown in Fig. 3. The neutron EOS is broken down into its four components; $c_n = 119$ MeV fm$^2$ is fixed by the Fermi-gas model, $d_n$ is relatively small, and the two most important parameters are $a_n$ and $b_n$. It is remarkable that the theoretical low-density EOS and the properties of doubly magic nuclei can all be understood with the Skyrme ansatz for the EDF (see also Ref. [3]). The two-parameter fit $a_n$ and $b_n$ to the three theoretical low-density neutron EOS points and the nuclear data is excellent for a reasonable range of the fixed values for the power of the density dependence $\gamma = 1 + \sigma$ and the effective-mass term $d_n$. As observed in Figs. 2 and 3, these three theoretical low-density points are sufficient to determine the shape of the EOS below $\rho_n = 0.04$ fm$^{-3}$.

Previously, theoretical properties of the neutron EOS were used to constrain the Skyrme parameters. For example, Chabanat *et al.* used microscopic calculations for neutron matter (Fig. 7 of Ref. [19]) up to $\rho_n = 1.5$ fm$^{-3}$ from Wiringa *et al.* [20] based on the Urbana 14 and Argonne $v_{14}$ $NN$ potential supplemented by the Urbana VII $3N$ potential. Brown [9] used the Friedman-Pandharipande neutron EOS [21] up to $\rho_n = 0.3$ fm$^{-3}$ (Fig. 2 in Ref. [9]). These calculations are no longer state of the art both considering the input $NN$ and $3N$ interactions as well as the many-body calculation. In contrast, our work focuses on low densities where the calculations and nuclear forces are well controlled. We take as constraint a conservative range at low densities based on modern QMC

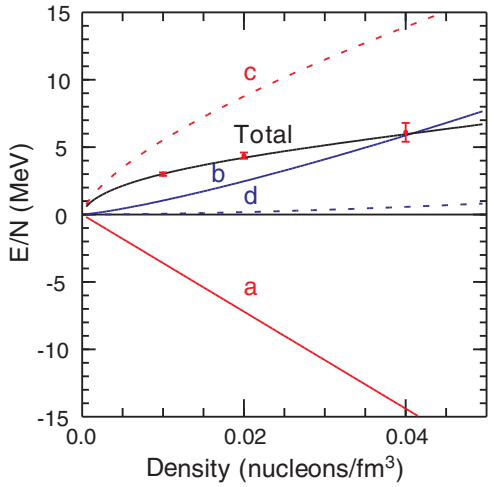


FIG. 3. (Color online) The neutron EOS at very low density. The total result for the Ska25 fit with a neutron-matter effective mass of 0.9 at a density of 0.10 fm$^{-3}$ is shown (black solid line) together with the separate contributions from the $a_n$ (red solid line), $b_n$ (blue solid line), $c_n$ (red dashed line), and $d_n$ (black dashed line) terms of Eq. (4). The theoretical data points are shown by the red points with error bars.

calculations as well as calculations based on systematic chiral EFT interactions.

There will be an uncertainty in the neutron EOS at high neutron density due to the dependence on $\sigma$ and the effective mass within the Skyrme EDFs. For our set of 12 EDFs and a range of $[m_n^*/m](\rho_n = 0.10\ \text{fm}^{-3}) = 0.9$–$1.1$, we obtain $[E/N](\rho_n = 0.32) = 37$–$51$ MeV.

It has been shown that the dipole polarizability of $^{208}$Pb is sensitive to the neutron skin of $^{208}$Pb [22] together with other properties of the neutron EOS [23,24]. The dipole polarizability of $^{208}$Pb recently was measured to be $\alpha_D = 20.1(6)\ \text{fm}^3$ [25]. The droplet model was used to obtain analytical relationships between $\alpha_D$, properties of the symmetry energy, and the surface properties of $^{208}$Pb [24]. If we use Eq. (11) from Ref. [24] together with the $J$ and $L$ values from the last row of Table I, we obtain $\alpha_D = 21.3(1.3)\ \text{fm}^3$. If we use Eq. (12) of Ref. [24] to obtain $R_{np}$ from $\alpha_D = 20.1(6)\ \text{fm}^3$ and $J = 33.2(20)$ MeV, we obtain $R_{np} = 0.188$ fm with an error of 0.009 that comes from Eq. (12) in Ref. [24] and an error of 0.011 that comes from the error in $J$. Thus, the present predictions are consistent with the measured dipole polarizability from Ref. [25]. Due to the constraints from doubly magic nuclei, our $^{208}$Pb neutron-skin prediction of 0.182(12) fm has a considerably tighter uncertainty compared to 0.17(3) fm from neutron-matter calculations only [26].

The $^{208}$Pb neutron-skin thickness can also be obtained from the lead radius experiment (PREX) using parity-violating electron scattering, which lead to $R_{np} = 0.302 \pm (0.175)_{\text{exp}} \pm (0.026)_{\text{model}} \pm (0.005)_{\text{strange}}$ fm [27,28]. A PREX-II experiment has been approved, that is expected to reduce the error bar to about 0.06 fm. This and the planned parity-violating experiments on $^{48}$Ca will be an important test of our predictions.

It will be important to see if any measured property is inconsistent with our predictions within their error range. If so, then a more complex form of the Skyrme functional would be inferred. Also, it will be important to carry out our analysis with other density-functional forms to see if the conclusions are robust. The present Skyrme EDFs provide a very useful starting point for new supernova EOSs.

This work was supported, in part, by the NSF Grant No. PHY-1068217, the Helmholtz Alliance Program of the Helmholtz Association, Contract No. HA216/EMMI "Extremes of Density and Temperature: Cosmic Matter in the Laboratory," and the ERC Grant No. 307986 STRONGINT. We thank the Institute for Nuclear Theory at the University of Washington for its hospitality.

[1] B. A. Brown, Phys. Rev. Lett. **85**, 5296 (2000); S. Typel and B. A. Brown, Phys. Rev. C **64**, 027302 (2001).
[2] A. W. Steiner, J. M. Lattimer, and E. F. Brown, Astrophys. J. **765**, L5 (2013).
[3] K. Hebeler, J. M. Lattimer, C. J. Pethick, and A. Schwenk, Astrophys. J. **773**, 11 (2013).
[4] M. Dutra, O. Lourenço, J. S. Sá Martins, A. Delfino, J. R. Stone, and P. D. Stevenson, Phys. Rev. C **85**, 035201 (2012).
[5] E. Chabanat, P. Bonche, P. Haensel, J. Meyer, and R. Schaeffer, Nucl. Phys. A **635**, 231 (1998).
[6] J. Bartel, P. Quentin, M. Brack, C. Guet, and H. B. Hakansson, Nucl. Phys. A **386**, 79 (1982).
[7] L. G. Cao, H. Sagawa, and G. Colo, Phys. Rev. C **86**, 054313 (2012).
[8] B. A. Brown, Phys. Rev. Lett. **111**, 232502 (2013).
[9] B. A. Brown, Phys. Rev. C **58**, 220 (1998).
[10] T. Krüger, I. Tews, K. Hebeler, and A. Schwenk, Phys. Rev. C **88**, 025802 (2013).
[11] I. Tews, T. Krüger, K. Hebeler, and A. Schwenk, Phys. Rev. Lett. **110**, 032504 (2013).
[12] K. Hebeler and A. Schwenk, Phys. Rev. C **82**, 014314 (2010).
[13] A. Gezerlis, I. Tews, E. Epelbaum, S. Gandolfi, K. Hebeler, A. Nogga, and A. Schwenk, Phys. Rev. Lett. **111**, 032501 (2013).
[14] E. Epelbaum, H. Krebs, D. Lee, and U.-G. Meißner, Eur. Phys. J. A **40**, 199 (2009); D. Lee (private communication).
[15] A. Akmal, V. R. Pandharipande, and D. G. Ravenhall, Phys. Rev. C **58**, 1804 (1998).
[16] S. Gandolfi, J. Carlson, and S. Reddy, Phys. Rev. C **85**, 032801(R) (2012); S. Gandolfi, J. Carlson, S. Reddy, A. W. Steiner, and R. B. Wiringa, arXiv:1307.5815.
[17] A. Schwenk, B. Friman, and G. E. Brown, Nucl. Phys. A **713**, 191 (2003).
[18] J. Carlson, S. Gandolfi, and A. Gezerlis, Prog. Theor. Exp. Phys. **1**, 01A209 (2012).
[19] E. Chabanat, P. Bonche, P. Haensel, J. Meyer, and R. Schaeffer, Nucl. Phys. A **627**, 710 (1997).

[20] R. B. Wiringa, V. Fiks, and A. Fabrocini, Phys. Rev. C **38**, 1010 (1988).
[21] B. Friedman and V. R. Pandharipande, Nucl. Phys. A **361**, 502 (1981).
[22] P. G. Reinhard and W. Nazarewicz, Phys. Rev. C **81**, 051303 (2010).
[23] J. Piekarewicz, B. K. Agrawal, G. Colò, W. Nazarewicz, N. Paar, P. G. Reinhard, X. Roca-Maza, and D. Vretenar, Phys. Rev. C **85**, 041302(R) (2012).
[24] X. Roca-Maza, M. Brenna, G. Colò, M. Centelles, X. Viñas, B. K. Agrawal, N. Paar, D. Vretenar, and J. Piekarewicz, Phys. Rev. C **88**, 024316 (2013).
[25] A. Tamii, I. Poltoratska, P. von Neumann-Cosel, Y. Fujita, T. Adachi, C. A. Bertulani, J. Carter, M. Dozono, H. Fujita, K. Fujita *et al*., Phys. Rev. Lett. **107**, 062502 (2011).
[26] K. Hebeler, J. M. Lattimer, C. J. Pethick, and A. Schwenk, Phys. Rev. Lett. **105**, 161102 (2010).
[27] PREX Collaboration, S. Abrahamyan, Z. Ahmed, H. Albataineh, K. Aniol, D. S. Armstrong, W. Armstrong, T. Averett, B. Babineau, A. Barbieri, and V. Bellini *et al*., Phys. Rev. Lett. **108**, 112502 (2012).
[28] C. J. Horowitz, Z. Ahmed, C.-M. Jen, A. Rakhman, P. A. Souder, M. M. Dalton, N. Liyanage, K. D. Paschke, K. Saenboonruang, R. Silwal *et al*., Phys. Rev. C **85**, 032501 (2012).